Photoacoustics 29 (2023) 100446

Contents lists available at ScienceDirect

Photoacoustics

journal homepage: www.elsevier.com/locate/pacs

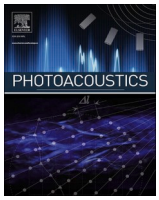

LED-based photoacoustic imaging for preoperative visualization of lymphatic vessels in patients with secondary limb lymphedema☆

Saskia Van Heumen [a,b], Jonas J.M. Riksen [b], Mithun Kuniyil Ajith Singh [c], Gijs Van Soest [b], Dalibor Vasilic [a,*]

[a] Department of Plastic and Reconstructive Surgery, Erasmus MC, University Medical Center, Rotterdam, the Netherlands
[b] Department of Cardiology, Erasmus MC, University Medical Center, Rotterdam, the Netherlands
[c] Research and Business Development Division, Cyberdyne Inc., Rotterdam, the Netherlands

ARTICLE INFO

Keywords:
Lymphedema
Photoacoustic Techniques
Extremities
Microsurgery
Lymphovenous Anastomosis
Lymphography
Fluorescence Imaging

ABSTRACT

Lymphedema is the accumulation of protein-rich fluid in the interstitium (i.e., dermal backflow (DBF)). Preoperative imaging of the lymphatic vessels is a prerequisite for lymphovenous bypass surgical planning. We investigated the visualization of lymphatic vessels and veins using light-emitting diode (LED)-based photoacoustic imaging (PAI).

Indocyanine-green mediated near-infrared fluorescence lymphography (NIRF-L) was done in fifteen patients with secondary limb lymphedema. Photoacoustic images were acquired in locations where lymphatic vessels and DBF were observed with NIRF-L.

We demonstrated that LED-based PAI can visualize and differentiate lymphatic vessels and veins even in the presence of DBF. We observed lymphatic and blood vessels up to depths of 8.3 and 8.6 mm, respectively.

Superficial lymphatic vessels and veins can be visualized using LED-based PAI even in the presence of DBF showing the potential for pre-operative assessment. Further development of the technique is needed to improve its usability in clinical settings.

1. Introduction

The lymphatic system is a network of tissues, vessels, and organs that fulfills several functions and is relatively poorly understood and understudied. The primary function is the transportation of interstitial fluids and proteins to the blood circulation while maintaining osmotic and hydrostatic pressure within the interstitial space [1]. The lymphatic system also plays a critical role in mediating the immune response and is the primary route for spread of tumor cells [2].

Small lymphatic capillaries initially collect the lymphatic fluid, which flows to the lymphatic trunks back to the circulatory system [3]. Two main factors contributing to adequate lymph flow are extrinsic/-passive forces (i.e., muscle contractions in the extremities, inflow pressure or outflow resistance) and intrinsic/active forces (i.e., lymphatic vessel contractions). Unidirectional valves divide the collecting lymphatic vessels into subsequent elementary pumping units and prevent backflow [4].

Dysfunction or obstruction of the lymphatic system impairs the essential transport function and can manifest in the formation of incompetent valves and buildup of the lymphatic fluid in the superficial dermal layer (i.e., dermal backflow (DBF)), causing lymphedema [4]. Secondary lymphedema is a common complication after surgical and radiotherapeutic treatment of cancer due to damage or obstruction of the lymphatic system. It is associated with severe discomfort and has a major impact on the quality of life [5]. Microsurgical lymphovenous bypass (LVB) surgery is increasingly performed when conventional treatments such as manual lymphatic drainage and compression garment therapy are not sufficient [6–9]. During the surgery, one or multiple lymphatic vessels are anastomosed to a nearby vein to bypass the site of lymphatic obstruction. Preoperative visualization of the lymphatic vessels, and ideally also of the veins, is of high importance to determine if the patient is eligible for this surgery and locate potential anastomosis sites.

A wide variety of imaging modalities have been used for this

☆ Trial registration: registered at trialregister.nl with trial registration number NL9595 and can be found on the International Clinical Trials Research Platform.

* Correspondence to: Department of Plastic and Reconstructive Surgery, Erasmus MC, University Medical Center, Doctor Molewaterplein 40, 3015 GD Rotterdam, the Netherlands.
E-mail address: d.vasilic@erasmusmc.nl (D. Vasilic).

https://doi.org/10.1016/j.pacs.2022.100446
Received 12 October 2022; Received in revised form 16 December 2022; Accepted 27 December 2022
Available online 28 December 2022

purpose. Lymphoscintigraphy gives an indication of the overall functioning of the lymphatics but the resolution is insufficient to localize anastomosis sites. On the other hand, magnetic resonance lymphography provides high-resolution images but is time consuming. Additional limitations of these techniques are high costs and lack of portability [10]. Near-infrared fluorescence lymphography (NIRF-L) has become popular and facilitates visualization of the lymphatic tracts and DBF in real-time using indocyanine green (ICG) contrast (see Fig. 1 for NIRF-L of healthy lymphatic vessels and DBF) [11–14]. Functional lymphatic vessels, which are suitable anastomosis sites, appear as linear structures, preferentially with visible pulsatility. However, NIRF-L has a relatively low resolution and cannot provide depth information, causing suboptimal decision-making in case of extensive DBF patterns [15–19]. NIRF-L also lacks the important ability to visualize suitable acceptor veins. Photoacoustic imaging (PAI) has properties that may overcome problems faced with NIRF-L [20,21]. PAI detects the acoustic signal generated by the thermoelastic response of a short light pulse that is absorbed by tissue, and forms an echo-like image of optical absorption at the illumination wavelength [22]. Both blood and the ICG injected for NIRF-L are strong absorbers and may thus be imaged by PAI [12,23].

Most PAI techniques use high-power laser-based systems with tunable wavelengths. These systems are bulky, complex, expensive, and require additional safety measures such as eye safety goggles and laser-safe rooms, hindering the clinical translation of PAI [24–26]. Substituting laser with light-emitting diode (LED) illumination overcomes these drawbacks. In recent years, developments in semiconductor technology have made it possible to fabricate high-power LED arrays for tissue illumination and thereby obtain sufficient image quality for clinical implementation of LED-based systems despite the lower light pulse energy [27,28].

PAI has shown its potential in multiple clinical applications such as the detection of joint inflammation [29,30], molecular imaging of oxidative stress[31], guiding minimally invasive procedures [32] and pathological angiogenesis on a small scale [33–35].

The purpose of this study was to explore the feasibility of dual-wavelength LED-based PAI for visualization of the lymphatic vessels and veins in secondary limb lymphedema, to improve pre-operative imaging for LVB surgical planning and assess the potential utility of PAI for determining suitable anastomosis sites. We compared the acquired data to NIRF-L images, knowing that the lack of depth information is a serious limitation of NIRF-L, which otherwise has many advantageous characteristics for preoperative imaging. We attempted to locate lymphatic structures observed with NIRF-L, and additionally identify veins that can serve as the acceptor site for the anastomosis. In addition, we investigated the feasibility of identifying lymphatic vessels in the presence of DBF.

There currently is no way to quantitatively establish the number of lymphatic vessels in vivo, owing to the complexity of the lymphatic network, variable contrast perfusion, and different factors influencing imaging resolution and sensitivity. Neither NIRF-L, nor PAI, is expected to visualize all vessels, and therefore a quantitative comparison of detection efficiency is presently not possible, and was not the objective of this study.

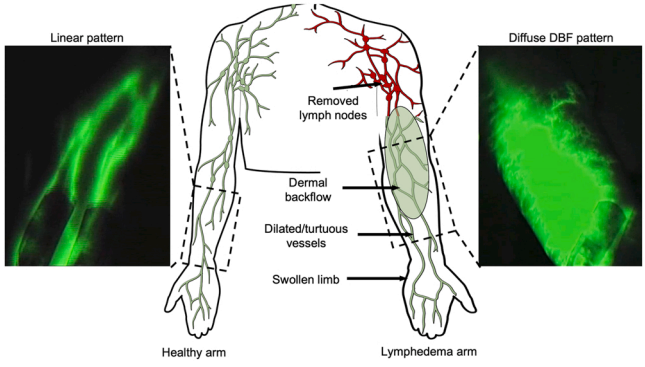

Fig. 1. Schematic on lymphedema and example indocyanine green mediated near-infrared fluorescence lymphography images of healthy lymphatic vessels and dermal backflow (DBF) often seen in lymphedema.

2. Methods

2.1. Patient population and study design

A prospective feasibility study of LED-based PAI in patients with secondary limb lymphedema was conducted from November 2021 until May 2022 at the Erasmus MC, University Medical Center Rotterdam (registered at trialregister.nl with trial registration number NL9595 and can be found on the International Clinical Trials Research Platform). A total of fifteen patients referred to the plastic- and reconstructive surgery department for (potential) microsurgical treatment of secondary limb lymphedema as a result of iatrogenic damage to the lymphatics were included. Exclusion criteria included iodine allergy, pregnancy, incapacity or bilateral lymphedema. If NIRF-L was not possible or failed, the patient was also excluded.

Patients were assessed in the outpatient clinic, followed by imaging on the same day. Demographics were collected including body mass index (BMI), age, surgical (cancer) treatment, radiation therapy, (neo) adjuvant chemotherapy, self-reported time since onset of lymphedema and in case of breast cancer, hormonal therapy. Patients were staged according to the International Society of Lymphology (ISL) grading system by an experienced plastic surgeon (DV) [36]. Circumference differences between the affected and healthy limb were measured on five different levels of both arms or legs (e.g., mid of the palm of the hand/foot, wrist/ankle, location on the forearm/lower leg with maximum symptomology, elbow/knee and location on the upper arm/leg with maximum symptomology).

2.2. Imaging protocol

First, NIRF-L videos from both extremities were acquired directly after ICG injection, according to regular protocol. Locations of observed linear pattern were indicated with a marker on both the healthy and affected limb as a control. Moreover, at least one location where a linear pattern transitioned into DBF was also marked. Directly after, combined ultrasound (US) and PAI was performed for a total duration of approximately 30 min. This protocol ensured that no additional ICG injections were necessary. Surgical decision-making was based solely on NIRF-L findings by the treating physician (DV), who assessed anonymized photoacoustic (PA) images only after surgery was performed to prevent influence in his surgical decision making.

2.2.1. Near-infrared fluorescence lymphography

NIRF-L videos were acquired using the Photodynamic Eye infrared camera system (Hamamatsu Photonics K.K., Hamamatsu, Japan), while using the fluorescence mapping function and varying the focus and excitation light intensity [13]. Prior to imaging ~0.2 mL ICG (0.25 % Verdye, Renew Pharmaceuticals Ltd, Ireland) was injected subcutaneously into all interdigital spaces of the affected limb and 2nd and 3rd interdigital spaces of the unaffected limb, following the local protocol. In some cases, variable locations such as the lateral/medial malleolus or lateral/medial sides of the wrist were injected additionally at the discretion of the treating physician. Injection sites were covered with adhesive bandages to prevent image saturation. Gentle massage was used to stimulate ICG flow. The images were classified according to the MD Anderson Cancer Center (MDACC) severity scale by an experienced plastic surgeon (DV) [37]. The entire procedure took ~30 min.

2.2.2. Photoacoustic imaging

Patients were imaged with the LED-based PAI system, Acoustic X

(Cyberdyne Inc., Tsukuba, Japan) operating with an US transducer (7 MHz, 80 % fractional bandwidth) and two high-density LED arrays intermittently emitting light at 820 nm (128 μJ) and 940 nm (114 μJ), with a pulse repetition frequency of 4 kHz and a pulse width of 70 ns. The overlap region of light from two LED arrays was approximately 36 mm × 3.5 mm (parallel x elevation), with a maximum fluence of 0.1 mJ/cm^2 and 0.09 mJ/cm^2 for 820 and 940 nm respectively, which is well below the maximum permissible exposure to optical radiation. A custom-made optically transparent coupling pad was used for acoustic coupling. Fig. 2 shows images of the device and the setup. The obtained image frames were averaged 640 times (64 frames averaged onboard in the DAQ and 10 frames in software), resulting in a final dual-wavelength frame rate of 6.25 Hz (combined PA and US). This resulted in image series with sufficient spatial contrast for dual-wavelength processing and interpretation, while preserving temporal resolution for probe positioning and visualizing dynamic phenomena. The system can obtain images with an axial and lateral resolution of 210 and 350 μm, respectively [28]. Both 2D (axial and parallel) and 3D images at multiple sites on the arm were acquired. 3D images were obtained by manually moving the probe with a linear motion over the region of interest while continuously acquiring axial images and rendered after the experiment using the built-in 3D software in the system.

2.3. Data processing

Patient demographics are reported using means and standard deviation. The NIRF-L videos and obtained images of the locations subsequently imaged with PAI were analyzed by two observers (SH and JR).

US and PA images were reconstructed using a built-in Fourier-based reconstruction software of the device using a sampling rate of 20 and 40 MHz for US and PA, respectively [38]. US images are displayed in grayscale and PA images in a pseudo color displayed superimposed on the US images. The first centimeter from the PA image was suppressed in the final visualization using the Acoustic X software since it only contains artefacts due to PA signal generated by the vibrations of the LEDs.

PA images resulting from 820 nm, 940 nm, 820 nm and 940 nm combined or 940/820 nm ratio can be displayed. Before applying the 940/820 nm ratio, the pixels are compensated for the difference in LED pulse energy at both wavelengths. The 940/820 nm ratio has been validated as a simple tool to differentiate ICG and blood in both phantom and in vivo studies on human volunteers[39,40] based on the absorption spectra of blood and ICG (see Fig. 3). Vessel detection was considered successful if a lymphatic vessel appeared as a stable feature in the images, and consensus was reached by the observers. Parallel images were considered successful if the path of a vessel could be followed for more than 3 mm, based on an estimate of the typical lymph tortuosity and the elevational image resolution. Success rates of imaging lymphatic vessels and blood vessels are reported separately as a percentage of imaged sites. If present, the depth of the detected lymphatic vessels and veins was measured using a built-in measurement function. From the 3D swipes, both the 2D axial slices as well as the maximum intensity projection (MIP) were generated and assessed. MIPs were created using both the 820 nm (ICG dominant) and 940 nm (blood dominant) signals and displayed superimposed in one image.

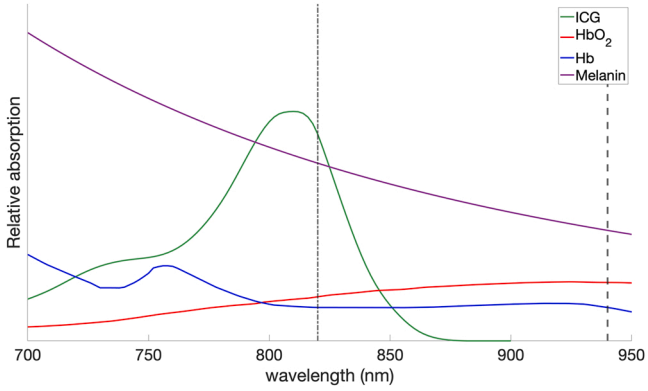

Fig. 3. Relative absorption spectra of indocyanine green (ICG), oxygenated hemoglobin (HbO2), deoxygenated hemoglobin (Hb) and melanin. Dotted lines represent wavelengths 820 and 940 nm.
Graphs reproduced from original data by Ref. [12] and digitized data from Ref. [64].

2.4. Study approval

All procedures complied with the Declaration of Helsinki and all measurements were performed at the Erasmus MC, University Medical Center, Rotterdam. The study is approved by the institutional medical ethics committee (NL78365.078.21). Written informed consent was obtained from all subjects prior to inclusion.

3. Results

3.1. Patient characteristics

Out of the fifteen patients, thirteen suffered from secondary lymphedema in the upper extremities, of which eleven were due to breast cancer treatment. In two patients the lower extremities were affected.

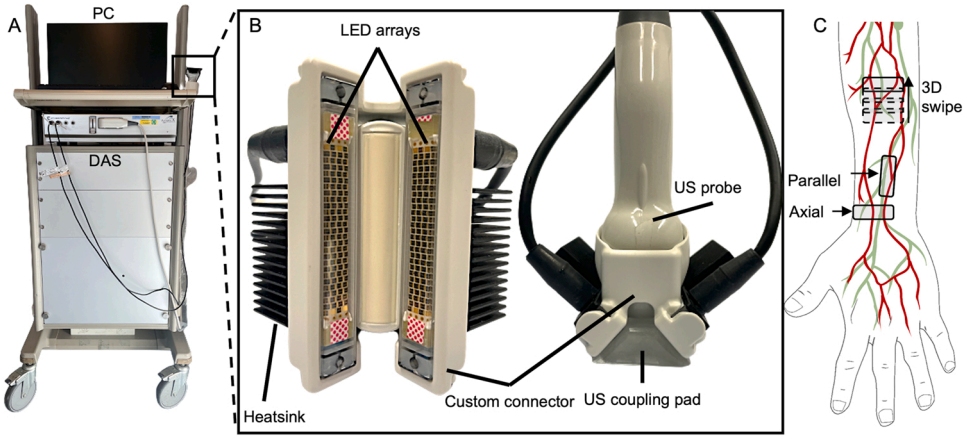

Fig. 2. (a) The Acoustic X system on a medical trolley. The system consists of a PC, data acquisition system (DAS), the ultrasound (US) probe and the light-emitting diode arrays (LEDs). (b) The LEDs are attached to the US probe with a custom connector. The custom US coupling pad is used for acoustic coupling with the imaged surface. (c) Schematic of different probe orientation used in this study for 2D and 3D data acquisition.

The majority of patients were classified as ISL stage 2 (73.3 %), one patient as stage 1 (6.7 %), and three patients as stage 3 (20 %). The average age and BMI were 53.3 ± 10.5 years and 26.8 ± 4.6 kg/m^2, respectively. The mean time since self-reported onset was 60.5 ± 52.8 months before their visit. Table 1 provides the detailed patient characteristics.

3.2. Imaging results

NIRF-L showed variable severities according to the MDACC staging, ranging from normal linear patterns only (stage 0) to severely obstructed lymphatics only showing diffuse dermal backflow patterns (stage IV).

PA images were acquired 35–45 min after ICG injection in locations with linear and DBF patterns. Fig. 4 shows the 820 nm, 940 nm, and 940/820 nm ratio PA images, acquired on the affected dorsal forearm in a location with linear flow observed with NIRF-L. A clear skin signal due to melanin absorption can be observed at both wavelengths. The optical absorption properties of blood cause a PA signal at both 820 nm and 940 nm, and therefore have a 940/820 nm ratio of ~1 (red in the ratio image). The measured blood vessels were identified as veins since arteries are located more deeply in the areas that were scanned and are easily distinguishable due to their pulsatility.

Lymphatic vessels result in a low 940/820 nm ratio (blue in the ratio image) because the ICG absorbs predominantly at 820. The ratio image provided simple and real-time information on vessel type and location.

Table 2 gives an overview of the NIRF-L and PAI findings for all patients. Lymphatic and blood vessels were imaged with axial and parallel orientation of the US probe. Lymphatic and blood vessels were observed at depths ranging between 0.5 and 8.3 mm and 0.5–8.6 mm from the skin surface, respectively. Overall, axial orientation of the probe produced more images in which lymphatic and blood vessels were identifiable compared to parallel orientation. A prolonged axial measurement of a lymphatic vessel is available as Supplementary Video 1. In cases with extensive DBF, lymphatic and blood vessels were successfully depicted in locations where NIRF-L did not show lymphatic vessels.

For three patients (i.e., numbers 11–13), a different (black) marker was used to indicate the lymphatic vessel locations. The use of this marker resulted in artefacts at an imaging depth where lymphatic vessels were expected. This resulted in an unreliable assessment and therefore these patients are excluded from the calculations for successful visualization.

We observed lymphatic vessels located close to or even beneath a blood vessel, a suitable bypass location (see Fig. 5). As mentioned, we could clearly distinguish signals from lymphatic and blood vessels in locations with DBF (see Fig. 6). However, there was no clear signature of DBF in the superficial PAI signal, due to ICG accumulation in the lymphatic capillaries or interstitium, while patently observed with NIRF-L. Fig. 7 shows a maximum intensity projection with two corresponding 2D axial images, resulting from an acquired 3D swipe. Video 2 shows the complete 3D swipe, which is available as supplementary information online.

Supplementary material related to this article can be found online at doi:10.1016/j.pacs.2022.100446.

4. Discussion

In this study, we assessed the feasibility of handheld LED-based PA visualization of lymphatic and blood vessels for LVB surgical planning in patients with secondary limb lymphedema.

PAI facilitated real-time visualization and differentiation of lymphatic vessels and veins using the 940/820 nm ratio functionality up to 8.6 mm depth. The ability to distinguish between these vessels with specific contrast is a significant advantage over solely (high-frequency) US imaging, because multiple US parameters such as shape, echogenic texture, doppler color, collapsibility and convergence need to be assessed to determine vessel type [41–44]. Recent studies have introduced contrast-enhanced US using microbubbles, increasing contrast for only the lymphatic vessels [45,46]. However, PAI provides contrast for both blood and lymphatic vessels in real-time. Additionally, ICG contrast-mediated imaging enables multi-modality (i.e., PAI and NIRF-L) imaging after a single injection.

Axial imaging yielded the most successful vessel detection. In most cases, lymphatic and blood vessels were visible within a couple of seconds of axial imaging. Similar to an US image acquisition, the lymphatic vessel can be followed to get an overview of the overall anatomy. Contrarily, parallel imaging of especially the lymphatic vessels was less straightforward. Small movements or angulation differences of the probe caused the image plane to change, leaving a small and sometimes tortuous lymphatic vessel partly outside the imaged frame. Similarly limited by imaging stability, no lymphatic vessel contractions were conclusively observed, because it was difficult to distinguish between PA signal changes due to probe and patient motion, or contractions. For

Table 1
Characteristics of the enrolled patients.

No.	Age (Years)	Sex	BMI (kg/m^2)	Clinical indication	Extremity	Duration (Months)	LND	Radiation therapy	Chemo therapy	ISL stage	Circ diff (%)
1	53	F	23.60	Breast cancer	A	80	+	+	+	3	12.0
2	54	F	32.87	Breast cancer	A	60	+ SLN only	+	+	2	2.5
3	45	F	20.53	Breast cancer	A	36	+	+	+	1	2.7
4	67	F	25.68	Breast cancer	A	60	+	+	+	2	3.6
5	44	F	20.34	Breast cancer	A	48	+	+	+	2	5.6
6	46	F	27.64	Breast cancer	A	14	+	+	-	2	3.4
7	57	F	29.02	Gastric bypass surgery	L	96	-	-	-	2	3.4
8	65	M	34.08	Sarcoma	A	24	-	+	-	3	10.7
9	62	F	28.67	Breast cancer	A	36	+	+	+	2	7.2
10	60	F	32.56	Breast cancer	A	39	+	+	+	2	6.2
11	69	F	24.80	Breast cancer	A	240	+	+	+	3	5.8
12	35	F	31.21	Breast cancer	A	18	+	+	+	2	3.7
13	33	F	26.57	Breast cancer	A	72	+	+	+	2	4.3
14	55	M	25.00	Melanoma	A	36	+	-	-	2	4.4
15	54	F	18.99	Cervical cancer	L	48	+	+	-	2	6.0
Average	53.3 ± 10.5		26.8 ± 4.6			60.5 ± 52.8					

F: female; M: male; BMI: body mass index; A: arm; L: leg; LND: lymph node dissection; SLN: sentinel lymph node; ISL: International Society of Lymphology; circ diff: circumference difference.

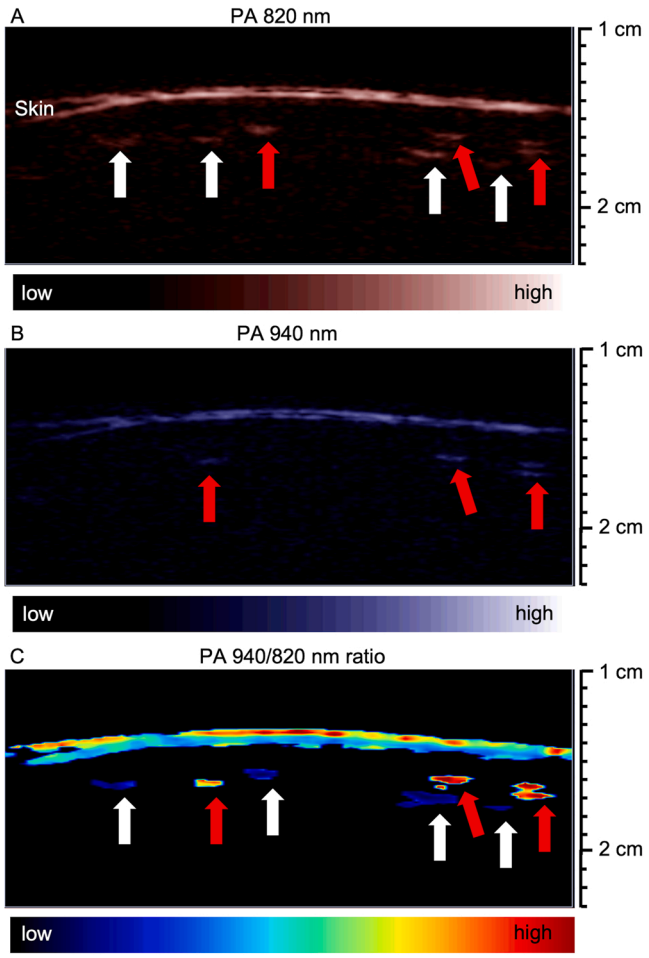

Fig. 4. Photoacoustic (PA) images of a patient with secondary arm lymphedema. Images represent a region with linear flow patterns on near-infrared fluorescence lymphography on the affected dorsal forearm. (A) PA signal from 820 nm light pulses. (B) PA signal from 940 nm light pulses. (C) 940/820 nm ratio image. White arrows indicate lymphatic vessels, for which the signal is absent in the 940 nm image. Red arrows indicate blood vessels resulting in signals at 820 and 940 nm. This results in a low ratio for lymphatic vessels (dark blue) and a ratio of ~1 (red) for blood vessels. The signal over the entire width between 13 and 15 mm depth (distance from ultrasound transducer) represents the skin.

example, the intensity variations shown in Video 1 could be due to any of these causes. Applying too much pressure can also result in compressing the vessels, pushing the ICG dye away from the imaging plane, which removes the necessary image contrast.

We also investigated the use of handheld 3D swipes for generating an overview of the joint course of lymphatic vessels and veins. Representation of the image as a MIP provides an approximate location of the structures of interest. During manual sweep acquisition, lateral motion and changes in probe moving speeds occur, whilst the 3D reconstruction algorithm does not account for this in its present implementation. Consequently, the resulting images can be affected by interpolation artefacts and unreliable distance information, complicating comparisons with NIRF-L images. Techniques such as probe tracking [47], tattoo tomography [48] or deep learning methods [49] could potentially improve 3D tomographic reconstructions. In addition, higher imaging frame rates could increase the 3D swipe quality.

Localization of DBF is an important clinically relevant finding for diagnosis and surgical planning. In this study, we observed that lymphatic vessels could be visualized with PAI in locations where extensive DBF obscured the vessels in NIRF-L images. This demonstrates a clear advantage of the depth resolution offered by PAI. In the data acquired to date, we were unable to identify a PA signal that can be attributed to DBF, likely because the ICG concentration in the superficial layer is low and there is a background absorption of melanin. Previous studies on PA visualization of the lymphatic system also described this phenomenon, especially when the contrast agent was present in low concentrations in the interstitium [50,51]. On the other hand, the minimal optical attenuation still leads to a strong NIRF-L signal due to DBF. Identification of such pathological patterns is an important diagnostic capability of NIRF-L and further research is required to investigate their PA appearance in more detail. Potential solutions might be multispectral imaging and spectral unmixing to differentiate further between tissue and contrast chromophores [52,53].

PAI has a limited imaging depth due to strong tissue optical absorption. However, in some cases, we observed more lymphatic vessels with PAI compared to NIRF-L. In patients with extensive edema or a higher BMI, lymphatic vessels might be too deep for sufficient visualization, especially in the proximal regions of the arm or leg. NIRF-L also suffers from this limitation, with maximum reported imaging depths of 1–1.5 cm [54].

Additionally, handheld PAI is still relatively operator dependent and less intuitive compared to NIRF-L. While NIRF-L provides a large field of view, providing an anatomical overview of the entire limb. PAI images a small field of view with high-resolution information, including depth information that is not limited by DBF.

PAI data may exhibit artefacts as a result of acoustic reflections of the generated PA wave [55,56]. Some of these reflection artefacts are easily identified, or show up at distances beyond the penetration depth of the excitation light, and can be cropped from the image. Reflection artefacts on bone surfaces have previously been demonstrated in imaging of the interphalangeal joints [57,58]. This artefact is more difficult to identify and could be confused for an actual lymphatic vessel. This emphasizes that users must have knowledge on the basic principles of PAI, to avoid misinterpretation. The anatomical information provided by the US images supports artefact identification and interpretability.

Several clinical laser-based systems such as the PAI-05 [59] and the iThera Medical MSOT Acuity [60,61] have also been used for lymphatic vessel imaging, producing high-resolution images. However, these systems are bulky or not portable at all, extra safety precautions are obligatory, and computationally intensive post-processing steps are needed [50,51,62]. This adds further challenges to the clinical implementation in multiple settings such as outpatient clinics and operating rooms. LED-based PAI overcomes these problems due to its portability and no required safety measures. Furthermore, reported imaging times with laser-based systems were long (120 min per limb), which would conflict with regular outpatient clinic schedules [60,61]. We demonstrated the possibility of acquiring extensive PAI images of both limbs within 30 min, which is compatible with a diagnostic consultation setting.

This study has some limitations. First, we did not assess the effect of skin melanin absorption on the ratio calculation. Greater optical absorption at 820 nm than at 940 nm could have led to spectral coloring, which was not accounted for in the computation of the ratio. Further investigations on spectral coloring effects on PA signal quantification and imaging depth should be done, especially for different levels of skin melanin.

Second, according to standard procedure, less ICG was injected in the healthy limb in contrast to the lymphedema limb. This could have influenced the success rate in the healthy limbs as a result of lower ICG concentrations. Since it is known that multi-lymphosome injections lead to more lymphatic vessels visualized with NIRF-L, it is likely that higher ICG concentrations in the lymphatic vessels and more injection locations will lead to easier visualization [63]. The ideal ICG concentration and injection locations for PAI are yet unknown.

Lastly, image acquisition and interpretation were done by the same observers (researchers with a background in Technical Medicine) for the

Table 2
MDACC staging of NIRF-L and number of PAI images that resulted in successful vessel detection (%).

No.	NIRF-L stage (MDACC)	No. of sites	Lymphatic vessel Detection (%)		Blood vessel detection (%)		Dominant DBF pattern	Lymphatic vessel visualized at DBF location	
			Axial	Parallel	Axial	Parallel		NIRF-L	PAI
1	II-III	4	75	25	100	25	Severe (D)	-	+
2	0	4	75*	25	100	100	Absent (L)	No DBF	No DBF
3	II	3	100	67	100	100	Severe (D)	-	+
4	II	4	75	50	100	50	Mild (Sd)	+	+
5	II	3	100	100	100	100	Mild (Sp)	+	+
6	II	3	67	100	100	67	Mild (Sp)	+	+
7	III	4	50	0	100	100	Severe (D)	-	+
8	II-III	3	100	100	100	100	Severe (D)	-	+
9	II	3	100	67	100	100	Mild (Sp)	+	+
10	II	4	75	100	100	100	Severe (D)	-	+
11[#]	II	3	-	-	-	-	Mild (Sp/Sd)	-	?[#]
12[#]	IV	3	-	-	-	-	Severe (D)	-	?[#]
13[#]	II	3	-	-	-	-	Mild (Sd)	+	?[#]
14	II	3	100	67	100	100	Severe (Sd/D)	-	+
15	I-II	3	33	33	100	100	Severe (D)	-	-
Total		**50**	**78**	**59**	**100**	**85**		5/11	10/11

*NIRF-L: near-infrared fluorescence lymphography; MDACC: MD Anderson Cancer Center; PAI: photoacoustic imaging; DBF: dermal backflow; L: linear; Sp: splash; Sd: stardust; D: diffuse. *In one of the four locations, no ICG signal was seen with NIRF-L. [#]black marker artefacts interfered with PA image assessment. These patients were not taken into account for successful vessel detection percentage calculations.*

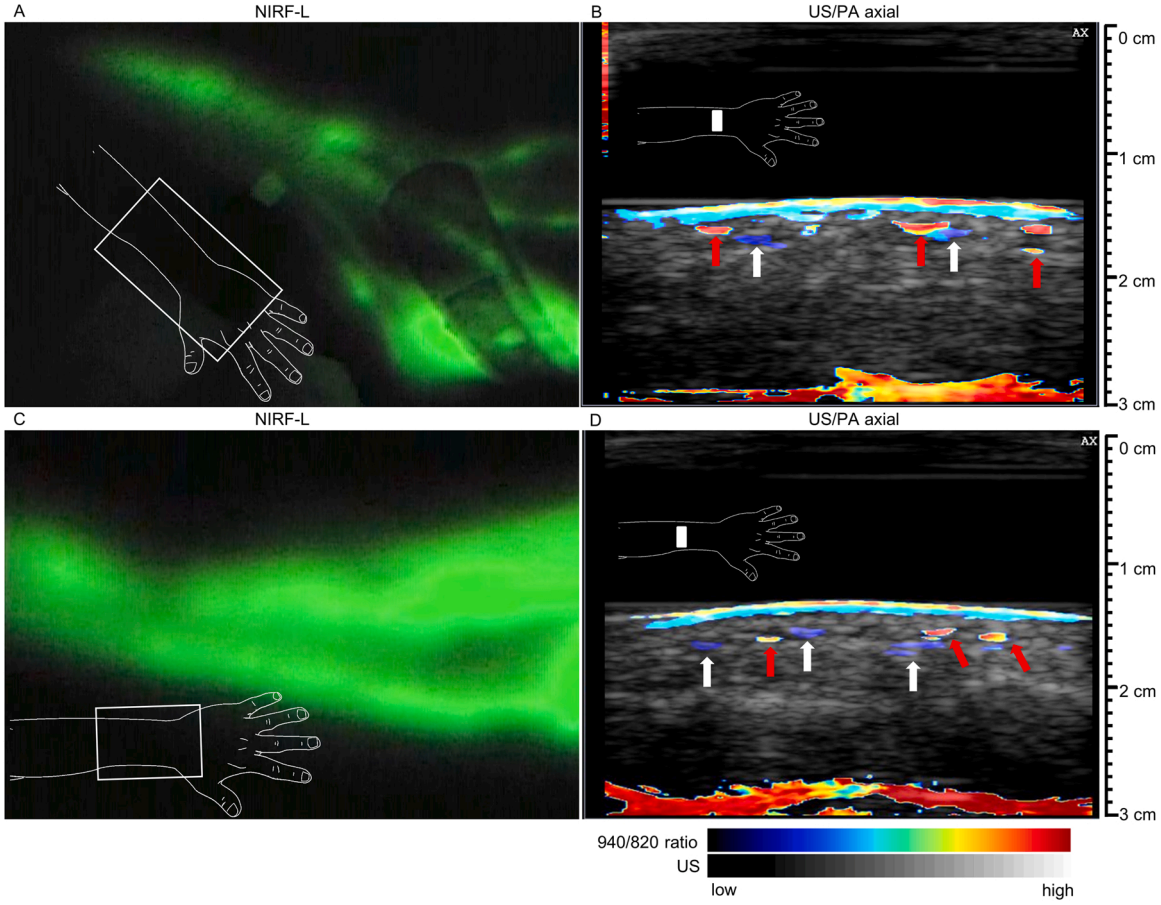

Fig. 5. Near-infrared fluorescence lymphography (NIRF-L) images (A and C) with linear patterns in a healthy arm (A) and lymphedema arm (C). B and C represent photoacoustic (PA) images of 940/820 nm ratio superimposed on grayscale ultrasound (US) images of the corresponding NIRF-L regions. Red arrows indicate blood vessels and white arrows indicate lymphatic vessels. More lymphatic vessels were observed with PA imaging compared to NIRF-L. Reflection artefacts originating from the skin surface can be observed at a depth of ~3 cm.

entire study. The effects of inter-observer variability of this technique are unknown and could potentially influence the imaging results.

5. Conclusions

Overall, we demonstrated that dual-wavelength, LED-based PAI can visualize lymphatic and blood vessels. In this study, we focused on the

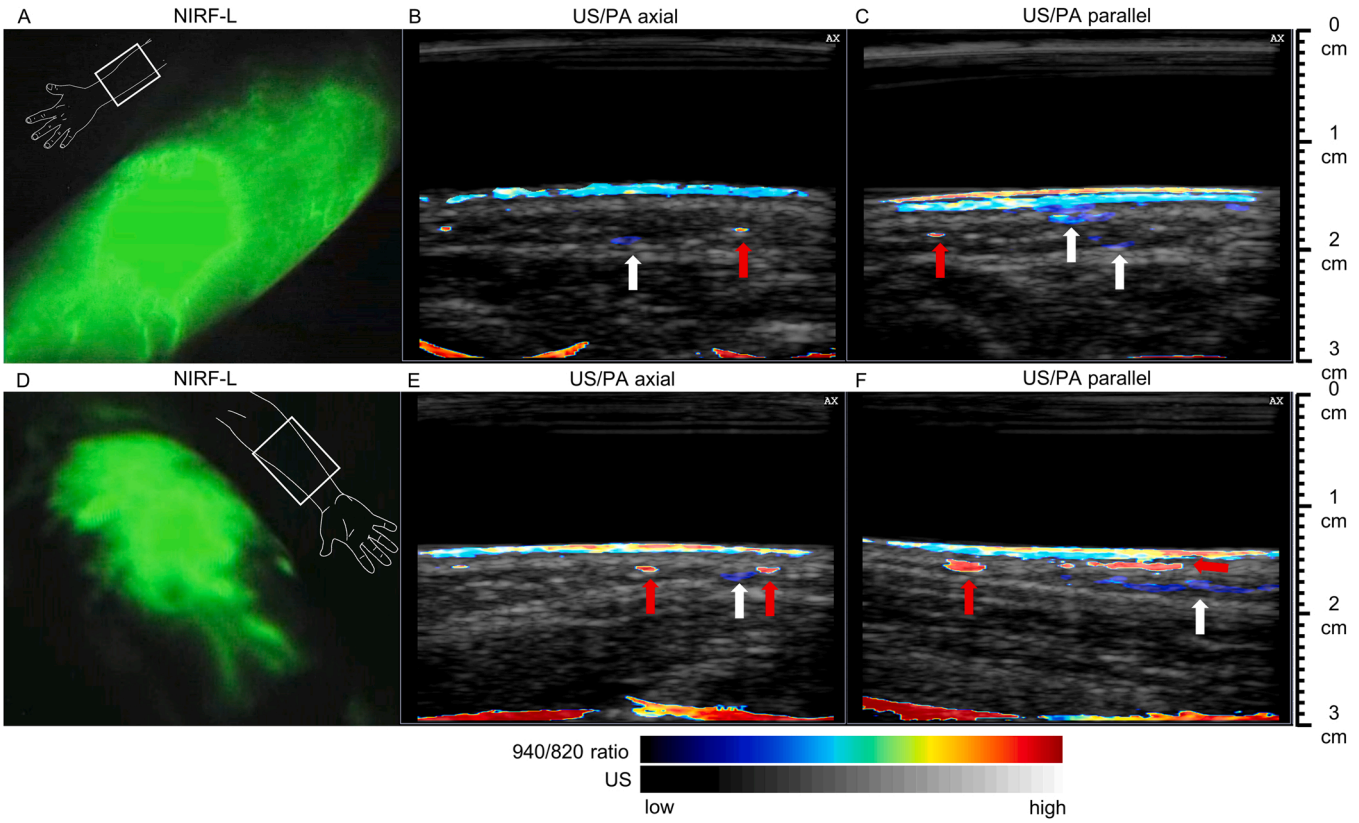

Fig. 6. Near-infrared fluorescence lymphography (NIRF-L) images (A, D) with extensive dermal backflow patterns and the corresponding axial (B, E) and parallel (C, F) 940/820 nm ratio photoacoustic (PA) images superimposed on grayscale ultrasound (US). Red arrows indicate blood vessels and white arrows indicate lymphatic vessels. In both cases, PA images were acquired in locations where no lymphatic vessels were observed with NIRF-L. Reflection artefacts originating from the skin surface can be observed at a depth of ~3 cm.

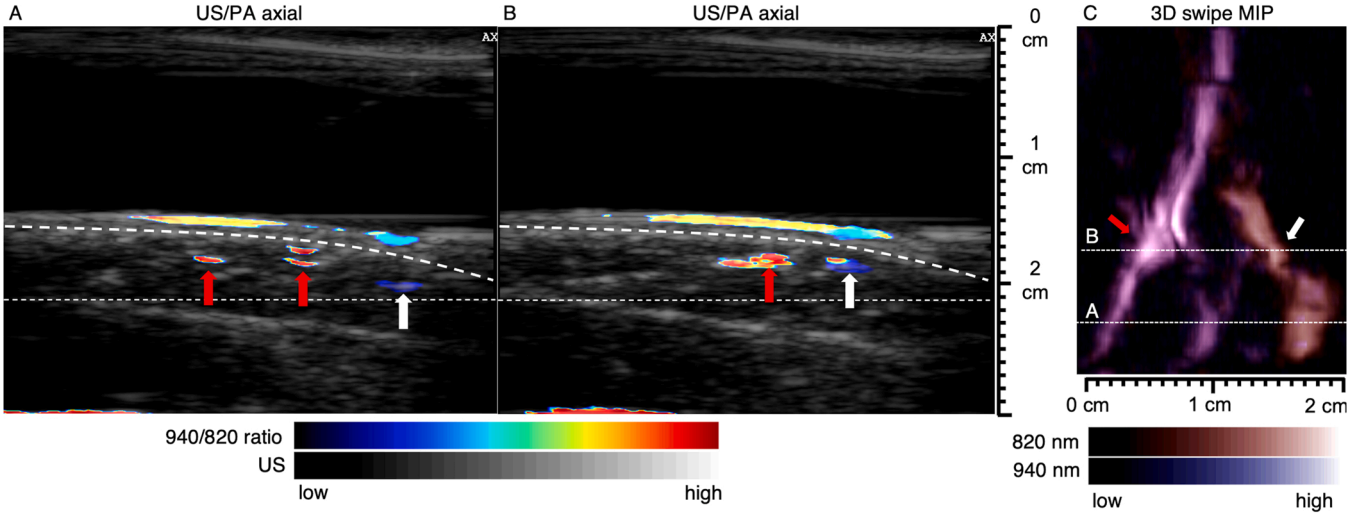

Fig. 7. A and B show axial photoacoustic (PA) images superimposed on grayscale ultrasound (US) from a 3D swipe. White dotted lines indicate the depth region, which was used for maximum intensity projection (MIP) image generation and fixed for all frames. Red arrows indicate blood vessels and white arrows indicate lymphatic vessels. C shows the resulting 3D swipe MIP of the overlaid 820 nm and 940 nm images, in total 1536 frames were used. The blood vessel that absorbs both wavelengths appears in pink and the lymphatic vessel in red.

application of LVB surgical planning, but the technique may also prove useful in imaging the superficial lymphatics for other lymphatic pathology such as metastasis patterns or systemic disease. For clinical translation of PAI to guide LVB surgical planning with the current workflow, it is important to have a compact and portable system. We showed that this novel technique can be used in a clinical setting and is not more invasive than NIRF-L, which is currently routinely used. These findings suggest that PAI has potential for preoperative lymphedema assessment, especially in cases with extensive DBF patterns hindering adequate assessment with NIRF-L. However, LED-based PAI is still in its early stages of development and technological advances are required to improve clinical usability, image quality, and minimize image artefacts.

CRediT authorship contribution statement

Saskia van Heumen: Conceptualization, Methodology, Formal Analysis, Investigation, Writing – Original Draft, Visualization, **Jonas Riksen:** Conceptualization, Methodology, Formal Analysis, Investigation, Writing – Review & Editing,**Mithun Kuniyil Ajith Singh:** Software, Resources, Writing – Review & Editing, **Gijs van Soest:** Conceptualization, Methodology, Investigation, Writing – Review & Editing, Supervision, **Dalibor Vasilic:** Conceptualization, Methodology, Writing – Review & Editing, Supervision.

Declaration of Competing Interest

The authors declare the following financial interests/personal relationships which may be considered as potential competing interests: Gijs van Soest reports equipment, drugs, or supplies was provided by Cyberdyne Inc. Saskia van Heumen reports equipment, drugs, or supplies was provided by Cyberdyne Inc. Jonas Riksen reports equipment, drugs, or supplies was provided by Cyberdyne Inc. Dalibor Vasilic reports equipment, drugs, or supplies was provided by Cyberdyne Inc. The research received in-kind support from Cyberdyne Inc. MKAS, who is an employee of Cyberdyne Inc., provided technical input for the design of the study and co-edited the manuscript. The company did not have any involvement in collection, analysis or interpretation of the data, or the decision to submit the manuscript for publication. The other authors declare that they have no known competing financial interests or personal relationships that could have appeared to influence the work reported in this paper.

Data Availability

The authors do not have permission to share data.

Acknowledgements

We thank the study participants for their time. We also thank the trial bureau for their input on the study approval process.

References

[1] M.A. Swartz, The physiology of the lymphatic system, Adv. Drug Deliv. Rev. 50 (1) (2001) 3–20, https://doi.org/10.1016/S0169-409X(01)00150-8.
[2] G.J. Randolph, S. Ivanov, B.H. Zinselmeyer, J.P. Scallan, The lymphatic system: integral roles in immunity, Annu Rev. Immunol. 35 (2017) 31–52, https://doi.org/10.1146/annurev-immunol-041015-055354.
[3] J.W. Breslin, Y. Yang, J.P. Scallan, R.S. Sweat, S.P. Adderley, W.L. Murfee, Lymphatic vessel network structure and physiology, Compr. Physiol. 9 (1) (2018) 207–299, https://doi.org/10.1002/cphy.c180015.
[4] J.P. Scallan, S.D. Zawieja, J.A. Castorena-Gonzalez, M.J. Davis, Lymphatic pumping: mechanics, mechanisms and malfunction, J. Physiol. 594 (20) (2016) 5749–5768, https://doi.org/10.1113/JP272088.
[5] N.R. Taghian, C.L. Miller, L.S. Jammallo, J. O'Toole, M.N. Skolny, Lymphedema following breast cancer treatment and impact on quality of life: a review, Crit. Rev. Oncol. Hematol. 92 (3) (2014) 227–234, https://doi.org/10.1016/j.critrevonc.2014.06.004.
[6] M.N. Basta, L.L. Gao, L.C. Wu, Operative treatment of peripheral lymphedema: a systematic meta-analysis of the efficacy and safety of lymphovenous microsurgery and tissue transplantation, Plast. Reconstr. Surg. 133 (4) (2014) 905–913, https://doi.org/10.1097/PRS.0000000000000010.
[7] D.W. Chang, H. Suami, R. Skoracki, A prospective analysis of 100 consecutive lymphovenous bypass cases for treatment of extremity lymphedema, Plast. Reconstr. Surg. 132 (5) (2013) 1305–1314, https://doi.org/10.1097/PRS.0b013e3182a4d626.
[8] M. Mihara, H. Hara, S. Tange, H.P. Zhou, M. Kawahara, Y. Shimizu, N. Murai, Multisite lymphaticovenular bypass using supermicrosurgery technique for lymphedema management in lower lymphedema cases, Plast. Reconstr. Surg. 138 (1) (2016) 262–272, https://doi.org/10.1097/PRS.0000000000002254.
[9] K. Rosian, M. Stanak, Efficacy and safety assessment of lymphovenous anastomosis in patients with primary and secondary lymphoedema: a systematic review of prospective evidence, Microsurgery 39 (8) (2019) 763–772, https://doi.org/10.1002/micr.30514.
[10] S. van Heumen, J.J.M. Riksen, W.M. Bramer, G. van Soest, D. Vasilic, Imaging of the lymphatic vessels for surgical planning: a systematic review, Ann. Surg. Oncol. (2022), https://doi.org/10.1245/s10434-022-12552-7.
[11] T. Desmettre, J.M. Devoisselle, S. Mordon, Fluorescence properties and metabolic features of indocyanine green (ICG) as related to angiography, Surv. Ophthalmol. 45 (1) (2000) 15–27, https://doi.org/10.1016/S0039-6257(00)00123-5.
[12] M.L. Landsman, G. Kwant, G.A. Mook, W.G. Zijlstra, Light-absorbing properties, stability, and spectral stabilization of indocyanine green, J. Appl. Physiol. 40 (4) (1976) 575–583, https://doi.org/10.1152/jappl.1976.40.4.575.
[13] T. Shikayama, Characteristics of the photodynamic eye camera, in: M. Kusano, N. Kokudo, M. Toi, M. Kaibori (Eds.), ICG Fluorescence Imaging and Navigation Surgery, Springer, Japan, Tokyo, 2016, pp. 21–27, https://doi.org/10.1007/978-4-431-55528-5_3.
[14] A.J.M. Cornelissen, T.J.M. van Mulken, C. Graupner, S.S. Qiu, X.H.A. Keuter, R.R.W.J. van der Hulst, R.M. Schols, Near-infrared fluorescence image-guidance in plastic surgery: a systematic review, Eur. J. Plast. Surg. 41 (3) (2018) 269–278, https://doi.org/10.1007/s00238-018-1404-5.
[15] H. Suami, A. Heydon-White, H. Mackie, S. Czerniec, L. Koelmeyer, J. Boyages, A new indocyanine green fluorescence lymphography protocol for identification of the lymphatic drainage pathway for patients with breast cancer-related lymphoedema, BMC Cancer 19 (1) (2019), https://doi.org/10.1186/s12885-019-6192-1.
[16] N. Unno, K. Inuzuka, M. Suzuki, N. Yamamoto, D. Sagara, M. Nishiyama, H. Konno, Preliminary experience with a novel fluorescence lymphography using indocyanine green in patients with secondary lymphedema, J. Vasc. Surg. 45 (5) (2007) 1016–1021, https://doi.org/10.1016/j.jvs.2007.01.023.
[17] T. Yamamoto, N. Matsuda, K. Doi, A. Oshima, H. Yoshimatsu, T. Todokoro, F. Ogata, M. Mihara, M. Narushima, T. Iida, I. Koshima, The earliest finding of indocyanine green lymphography in asymptomatic limbs of lower extremity lymphedema patients secondary to cancer treatment: the modified dermal backflow stage and concept of subclinical lymphedema, Plast. Reconstr. Surg. 128 (4) (2011) 314e–321e.
[18] T. Yamamoto, M. Narushima, K. Doi, A. Oshima, F. Ogata, M. Mihara, I. Koshima, G.S. Mundinger, Characteristic indocyanine green lymphography findings in lower extremity lymphedema: the generation of a novel lymphedema severity staging system using dermal backflow patterns, Plast. Reconstr. Surg. 127 (5) (2011) 1979–1986.
[19] T. Yamamoto, N. Yamamoto, K. Doi, A. Oshima, H. Yoshimatsu, T. Todokoro, F. Ogata, M. Mihara, M. Narushima, T. Iida, I. Koshima, Indocyanine green-enhanced lymphography for upper extremity lymphedema: a novel severity staging system using dermal backflow patterns, Plast. Reconstr. Surg. 128 (4) (2011) 941–947.
[20] H. Kajita, Y. Suzuki, H. Sakuma, N. Imanishi, T. Tsuji, M. Jinzaki, S. Aiso, K. Kishi, Visualization of Lymphatic Vessels Using Photoacoustic Imaging, Keio J. Med (2020) 1–11, https://doi.org/10.2302/kjm.2020-0010-oa.
[21] A.P. Lillis, R. Krishnamurthy, Photoacoustic imaging addresses a long-standing challenge in lymphedema, Radiology 295 (2) (2020) 475–477, https://doi.org/10.1148/radiol.2020192824.
[22] L.V. Wang, Tutorial on photoacoustic microscopy and computed tomography, IEEE J. Sel. Top. Quant. Elec 14 (1) (2008) 171–179, https://doi.org/10.1109/JSTQE.2007.913398.
[23] S. Han, D. Lee, S. Kim, H.H. Kim, S. Jeong, J. Kim, Contrast agents for photoacoustic imaging: a review focusing on the wavelength range, Biosens. (Basel) 12 (8) (2022), https://doi.org/10.3390/bios12080594.
[24] H. Zhong, T. Duan, H. Lan, M. Zhou, F. Gao, Review of low-cost photoacoustic sensing and imaging based on laser diode and light-emitting diode, Sensors (Basel) 18 (7) (2018) 2264, https://doi.org/10.3390/s18072264.
[25] Y. Zhu, T. Feng, Q. Cheng, X. Wang, S. Du, N. Sato, M. Kuniyil Ajith Singh, J. Yuan, Towards clinical translation of LED-based photoacoustic imaging: a review, Sensors (Basel) 20 (9) (2020) 2484, https://doi.org/10.3390/s20092484.
[26] Y. Zhu, G. Xu, J. Yuan, J. Jo, G. Gandikota, H. Demirci, T. Agano, N. Sato, Y. Shigeta, X. Wang, Light emitting diodes based photoacoustic imaging and potential clinical applications, 9885-9885, Sci. Rep. 8 (1) (2018), https://doi.org/10.1038/s41598-018-28131-4.
[27] T. Agano, N. Sato, K. Awazu, LED-based photoacoustic imaging system: why it achieves the same signal to noise ratio as solid-state-laser-based system: a review, in: SPIE BiOS, 11240, 2020, https://doi.org/10.1117/12.2544486.
[28] S. Agrawal, M. Kuniyil Ajith Singh, K. Johnstonbaugh, D.C. Han, C.R. Pameijer, S.-R. Kothapalli, Photoacoustic imaging of human vasculature using LED versus laser illumination: a comparison study on tissue phantoms and in vivo humans, Sensors 21 (2) (2021) 424.
[29] J. Jo, G. Xu, E. Schiopu, D. Chamberland, G. Gandikota, X. Wang, Imaging of enthesitis by an LED-based photoacoustic system, J. Biomed. Opt. 25 (12) (2020), 126005.
[30] J. Jo, G. Xu, Y. Zhu, M. Burton, J. Sarazin, E. Schiopu, G. Gandikota, X. Wang, Detecting joint inflammation by an LED-based photoacoustic imaging system: a feasibility study, J. Biomed. Opt. 23 (11) (2018) 1–4, https://doi.org/10.1117/1.JBO.23.11.110501.
[31] A. Hariri, E. Zhao, A.S. Jeevarathinam, J. Lemaster, J. Zhang, J.V. Jokerst, Molecular imaging of oxidative stress using an LED-based photoacoustic imaging system, 11378-11378, Sci. Rep. 9 (1) (2019), https://doi.org/10.1038/s41598-019-47599-2.
[32] W. Xia, M. Kuniyil Ajith Singh, E. Maneas, N. Sato, Y. Shigeta, T. Agano, S. Ourselin, S.J. West, A.E. Desjardins, Handheld real-time LED-based photoacoustic and ultrasound imaging system for accurate visualization of clinical metal needles and superficial vasculature to guide minimally invasive procedures, Sens. (Basel) 18 (5) (2018) 1394, https://doi.org/10.3390/s18051394.
[33] A.B.E. Attia, G. Balasundaram, M. Moothanchery, U.S. Dinish, R. Bi, V. Ntziachristos, M. Olivo, A review of clinical photoacoustic imaging: current and

future trends, 100144-100144, Photoacoustics 16 (2019), https://doi.org/10.1016/j.pacs.2019.100144.
[34] M. Xavierselvan, M.K. Singh, S. Mallidi, In vivo tumor vascular imaging with light emitting diode-based photoacoustic imaging system, 4503-4503, Sensors 20 (16) (2020), https://doi.org/10.3390/s20164503.
[35] H. Zhang, G. Zhang, Y. Zhang, L. Wen, M. Zhang, J. Pan, P. Wang, X. Wang, Q. Cheng, X. Wang, Quantitatively assessing port-wine stains using a photoacoustic imaging method: a pilot study, 33183-2, J. Am. Acad. Dermatol. S0190–9622 (20) (2021), https://doi.org/10.1016/j.jaad.2020.12.024.
[36] International Society of Lymphology, The diagnosis and treatment of peripheral lymphedema: 2016 consensus document of the International Society of Lymphology, Lymphology 49 (4) (2016) 170–184.
[37] A.T. Nguyen, H. Suami, M.M. Hanasono, V.A. Womack, F.C. Wong, E.I. Chang, Long-term outcomes of the minimally invasive free vascularized omental lymphatic flap for the treatment of lymphedema, J. Surg. Oncol. 115 (1) (2017) 84–89, https://doi.org/10.1002/jso.24379.
[38] M. Jaeger, S. Schüpbach, A. Gertsch, M. Kitz, M. Frenz, Fourier reconstruction in optoacoustic imaging using truncated regularized inverse k -space interpolation, Inverse Probl. 23 (6) (2007) S51–S63, https://doi.org/10.1088/0266-5611/23/6/s05.
[39] M. Kuniyil Ajith Singh, T. Agano, N. Sato, Y. Shigeta, T. Uemura, Real-time in vivo imaging of human lymphatic system using an LED-based photoacoustic/ultrasound imaging system. SPIE BiOS, 2018, https://doi.org/10.1117/12.2290871.
[40] Anon
[41] M. Czedik-Eysenberg, J. Steinbacher, B. Obermayer, H. Yoshimatsu, H. Hara, M. Mihara, C.H.J. Tzou, S. Meng, Exclusive use of ultrasound for locating optimal LVA sites—a descriptive data analysis, J. Surg. Oncol. 121 (1) (2020) 51–56, https://doi.org/10.1002/jso.25728.
[42] A. Hayashi, N. Hayashi, H. Yoshimatsu, T. Yamamoto, Effective and efficient lymphaticovenular anastomosis using preoperative ultrasound detection technique of lymphatic vessels in lower extremity lymphedema, J. Surg. Oncol. 117 (2) (2018) 290–298, https://doi.org/10.1002/jso.24812.
[43] A. Hayashi, T. Yamamoto, H. Yoshimatsu, N. Hayashi, M. Furuya, M. Harima, M. Narushima, I. Koshima, Ultrasound visualization of the lymphatic vessels in the lower leg, Microsurgery 36 (5) (2016) 397–401.
[44] M. Mihara, H. Hara, Y. Kawakami, Ultrasonography for classifying lymphatic sclerosis types and deciding optimal sites for lymphatic-venous anastomosis in patients with lymphoedema, J. Plast. Reconstr. Aesthet. Surg. 71 (9) (2018) 1274–1281.
[45] O. Lahtinen, R. Vanninen, S. Rautiainen, Contrast-enhanced ultrasound: a new tool for imaging the superficial lymphatic vessels of the upper limb, Eur. Radiol. Exp. 6 (1) (2022), https://doi.org/10.1186/s41747-022-00270-4.
[46] S. Jang, C.U. Lee, G.K. Hesley, J.M. Knudsen, N.J. Brinkman, N.V. Tran, Lymphatic mapping using US microbubbles before Lymphaticovenous anastomosis surgery for lymphedema, Radiology (2022), 212351, https://doi.org/10.1148/radiol.212351.
[47] S. Sun, B.W. Anthony, Freehand 3D ultrasound volume imaging using a miniature-mobile 6-DOF camera tracking system, 9th IEEE Int. Symp. Biomed. Imaging (ISBI) (2012) 1084–1087, https://doi.org/10.1109/ISBI.2012.6235747.
[48] N. Holzwarth, M. Schellenberg, J. Gröhl, K. Dreher, J.-H. Nölke, A. Seitel, M. D. Tizabi, B.P. Müller-Stich, L. Maier-Hein, Tattoo tomography: Freehand 3D photoacoustic image reconstruction with an optical pattern, Int J. Comput. Assist Radio. Surg. 16 (7) (2021) 1101–1110, https://doi.org/10.1007/s11548-021-02399-w.
[49] R. Prevost, M. Salehi, S. Jagoda, N. Kumar, J. Sprung, A. Ladikos, R. Bauer, O. Zettinig, W. Wein, 3D freehand ultrasound without external tracking using deep learning, Med. Image Anal. 48 (2018) 187–202, https://doi.org/10.1016/j.media.2018.06.003.
[50] Y. Suzuki, H. Kajita, A. Oh, M. Urano, S. Watanabe, H. Sakuma, N. Imanishi, T. Tsuji, M. Jinzaki, K. Kishi, Photoacoustic lymphangiography exhibits advantages over near-infrared fluorescence lymphangiography as a diagnostic tool in patients with lymphedema, e1, J. Vasc. Surg. Venous Lymphat. Disord. 10 (2) (2022) 454–462, https://doi.org/10.1016/j.jvsv.2021.07.012.
[51] A. Oh, H. Kajita, N. Imanishi, H. Sakuma, Y. Takatsume, K. Okabe, S. Aiso, K. Kishi, Three-dimensional analysis of dermal backflow in cancer-related lymphedema using photoacoustic lymphangiography, Arch. Plast. Surg. 49 (1) (2022) 99–107, https://doi.org/10.5999/aps.2021.01235.
[52] S. Agrawal, C. Fadden, A. Dangi, X. Yang, H. Albahrani, N. Frings, S. Heidari Zadi, S.-R. Kothapalli, Light-emitting-diode-based multispectral photoacoustic computed tomography system, Sensors 19 (22) (2019), https://doi.org/10.3390/s19224861.
[53] V. Grasso, J. Holthof, J. Jose, An automatic unmixing approach to detect tissue chromophores from multispectral photoacoustic imaging, Sensors 20 (11) (2020), https://doi.org/10.3390/s20113235.
[54] A.K. Polomska, S.T. Proulx, Imaging technology of the lymphatic system, Adv. Drug Deliv. Rev. 170 (2021) 294–311, https://doi.org/10.1016/j.addr.2020.08.013.
[55] M. Jaeger, J.C. Bamber, M. Frenz, Clutter elimination for deep clinical optoacoustic imaging using localised vibration tagging (LOVIT), Photoacoustics 1 (2) (2013) 19–29, https://doi.org/10.1016/j.pacs.2013.07.002.
[56] M. Kuniyil Ajith Singh, M. Jaeger, M. Frenz, W. Steenbergen, Photoacoustic reflection artifact reduction using photoacoustic-guided focused ultrasound: Comparison between plane-wave and element-by-element synthetic backpropagation approach, Biomed. Opt. Express 8 (2017) 2245–2260, https://doi.org/10.1364/BOE.8.002245.
[57] E. Peter van, K.B. Samir, J.B.M. Hein, S. Wiendelt, M. Srirang, Initial results of finger imaging using photoacoustic computed tomography, J. Biomed. Opt. 19 (6) (2014) 1–3, https://doi.org/10.1117/1.JBO.19.6.060501.
[58] H.N.Y. Nguyen, A. Hussain, W. Steenbergen, Reflection artifact identification in photoacoustic imaging using multi-wavelength excitation, Biomed. Opt. Express 9 (10) (2018) 4613–4630, https://doi.org/10.1364/BOE.9.004613.
[59] K. Nagae, Y. Asao, Y. Sudo, N. Murayama, Y. Tanaka, K. Ohira, Y. Ishida, A. Otsuka, Y. Matsumoto, S. Saito, M. Furu, K. Murata, H. Sekiguchi, M. Kataoka, A. Yoshikawa, T. Ishii, K. Togashi, T. Shiina, K. Kabashima, T. Yagi, Real-time 3D photoacoustic visualization system with a wide field of view for imaging human limbs, F1000Research 7 (2019) 1813, https://doi.org/10.12688/f1000research.16743.2.
[60] L. Grünherz, E. Gousopoulos, C. Barbon, S. Uyulmaz, B. Lafci, D. Razansky, A. Boss, P. Giovanoli, N. Lindenblatt, Preoperative mapping of lymphatic vessels by multispectral optoacoustic tomography, Lymphat. Res. Biol. (2022), https://doi.org/10.1089/lrb.2021.0067.
[61] G. Giacalone, T. Yamamoto, F. Belva, A. Hayashi, Bedside 3D visualization of lymphatic vessels with a handheld multispectral optoacoustic tomography device, 815-815, J. Clin. Med. 9 (3) (2020), https://doi.org/10.3390/jcm9030815.
[62] Y. Suzuki, H. Kajita, S. Watanabe, M. Otaki, K. Okabe, H. Sakuma, Y. Takatsume, N. Imanishi, S. Aiso, K. Kishi, Surgical applications of lymphatic vessel visualization using photoacoustic imaging and augmented reality, J. Clin. Med. 11 (1) (2022) 194, https://doi.org/10.3390/jcm11010194.
[63] H. Hara, M. Mihara, Multi-area lymphaticovenous anastomosis with multi-lymphosome injection in indocyanine green lymphography: a prospective study, Microsurgery 39 (2) (2019) 167–173, https://doi.org/10.1002/micr.30398.
[64] S. Prahl. Optical Absorption of Indocyanine Green (ICG). Accessed 20–08-2021, 2021. ⟨https://omlc.org/spectra/icg/⟩.

Saskia van Heumen obtained her Bachelor's degree in Clinical Technology from Delft, University of Technology in 2017. She obtained a postgraduate diploma in Medical Physics from University College London in 2018 and finalized her Master's degree in Technical Medicine at Delft, University of Technology in 2021. She carried out research on LED-based photoacoustic imaging for imaging of the lymphatic vessels as part of her master thesis project at the department of Plastic- and Reconstructive Surgery and the Biomedical Engineering Department at the Erasmus MC, University Medical Center in Rotterdam.

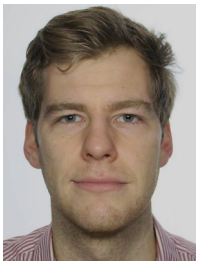

Jonas Riksen is a Technical Physician and PhD student in the research group of Gijs van Soest, in the Dept. of Cardiology at the Erasmus MC. He graduated in 2020 from the master's program Technical Medicine – Medical Imaging & Intervention at the University of Twente, which has an innovative role in the field of technical-medical diagnosis and treatment. His current research mainly involves around in vivo photoacoustic imaging of carotid artery atherosclerosis.

Mithun Kuniyil Ajith Singh is an engineering scientist with extensive experience in preclinical and clinical photoacoustic and ultrasound imaging. He is presently working as a research and business development manager at CYBERDYNE INC. in the Netherlands. In his current role, he initiates and coordinates various scientific projects in collaboration with globally renowned research groups, especially focusing on the clinical translation of LED-based photoacoustic imaging technology. Mithun earned his doctorate in 2016 from the University of Twente in the Netherlands under the supervision of professor Wiendelt Steenbergen. Mithun has published multiple international journal articles and book chapters, mainly focused on accelerating the translation of photoacoustic imaging from bench to bedside. He is the editor of LED-Based Photoacoustic Imaging, the first book on the topic, published by Springer Nature in 2020.

Gijs van Soest is a Professor in the Dept. of Cardiology at Erasmus MC, and leads the research group, part of the Biomedical Engineering lab, that specializes in the development of catheter-based and endoscopic imaging technologies based on light, ultrasound, and combinations thereof. Trained as an experimental physicist (MSc University of Groningen 1997, PhD University of Amsterdam 2001), he worked on atmospheric remote sensing before dedicating himself to interventional imaging in cardiology. He is a founder of Kaminari Medical, a company developing intravascular photoacoustic imaging. He is also a scientific director and founder of the biannual Optics in Cardiology conference.

Dalibor Vasilic studied medicine at Erasmus University and was trained as a plastic surgeon at University Hospital Utrecht. He defended his thesis on facial transplantation - composite tissue allotransplantation (CTA) that has helped move this field from bench to bedside resulting in first transplantation of human face. Dr. Vasilic is a EUROPEAN BOARD- certified microsurgeon and he leads the clinical and research line dedicated to pathology of lymphatic system as a consequence of oncological disease and has pioneered the (supra)microsurgical treatments of lymphedema. He founded the supramicorsurgical unit for treatment of cancer related lymphedema, which he now leads at the ErasmusMC.